Anisotropic and Nonlinear Mechanical Properties in Two-dimensional Nanomaterials

Ming Yu[1],*, Congyan Zhang[1], Safia Abdullah R Alharbi[1], Anna Zeng[2], Kevin Zeng[3], Emily Liu[4]

[1]*Department of Physics and Astronomy, University of Louisville, Louisville, Kentucky, 40292 USA*
[2]*Department of Computer Science, Massachusetts Institute of Technology, Cambridge, MA, 02139 USA*
[3]*Department of Computer Science, Columbia University, New York, NY, 10027 USA*
[4]*DuPont Manual High School, 120 W. Lee St, Louisville, Kentucky, 40208 USA*

*Corresponding author: E-mail: m0yu0001@louisville.edu; Tel: (01) 502-852-0931

Abstract

A systematic computational calculation based on the state-of-the-art quantum mechanics mothed was carried out to study the response of mechanical properties to various strains exerted on graphene, SiC sheet, and recently predicted two-dimensional (2D) sandwiched GaP and InP binary compounds. It was found that these 2D materials undergo an elastic expansion, a structural deformation, and then a structural broken process as the strain increases. Such process strongly depends on the direction of the strain exerted on 2D materials. In particular, a phase transition occurs in 2D sandwiched GaP and InP binary compounds when the strain exerts in zigzag direction. Calculated mechanical properties show that graphene has large linear and nonlinear elastic moduli, followed by 2D SiC monolayer. While the sandwiched GaP and InP structures possess significant anisotropic and nonlinear mechanical properties. Especially, those constants in the zigzag direction are about three to nine times greater than that in the armchair direction. Compared to graphene, they are softer, even along the zigzag direction. Such results provide fundamental information at atomic level for synthesizing, designing, and fabricating nanoelectromechanical and nanoelectronic devices. Copyright © VBRI Press.

Keywords: Mechanical properties, anisotropic behavior, Young's modulus, nonlinear elastic modulus.

Introduction

Extensive researches have focused on two-dimensional (2D) materials since the first synthesis of graphene in 2004 [**1-3**]. Hexagonal BN (h-BN) was discovered soon after the discovery of the graphene [**4, 5**], followed by 2D single element (such as silicene and germanene [**6**]) and transition-metal dichalcogenides (TMD) around 2010 [**7-9**]. In 2014, a novel 2D material, phosphorene was successfully synthesized [**10-12**]. Up to now, various new types of 2D materials have been discovered including MXenes [**13, 14**], 2D metals [**15**], 2D metal-oxides [**16**], layered double hydroxides [**17**], covalent organic frameworks (COFs) [**18**], and metal-organic-frameworks (MOFs) [**19**]. In additional to the diversity in their structural properties, their electronic properties are also diverse, from insulator to semiconductor, half-metal, semimetal, metal, and superconductor [**20**], which promise extensive applications in nanoelectronics, optics, printed sensors, electrolytes, energy storage, solar cells, etc. [**21, 22**].

2D materials also exhibit unique mechanical properties. In particular, with the discovery of outstanding mechanical strength and toughness of graphene (*i.e.*, its stiffness of 1 TPa is almost 100 times greater than a hypothetical steel film of the same thickness) [**23**], mechanical properties of 2D nanomaterials have been of major interest to material scientists and engineers [**24**]. Various experimental tools are used to test 2D mechanical properties including nanoindentation [**25**], MEM-based mechanical test [**26, 27**], Bulge test [**28, 29**], in-situ TEM observation [**30**], Raman spectroscopy [**31**], shearing test by probe tip [**32, 33**], miniaturized ballistic test [**34**], and Friction-force microscopy [**35-37**]. Although many experimental measurements have been performed, fundamental researches on the intrinsic mechanical properties of ultrathin 2D materials is still challenge and are keys to understand how the 2D materials response to strains induced from the material growth and deformations induced from processing them into nanodevice. Theoretical and numerical methods are very effective for either predicting mechanical behaviors or validating experimental results and are indeed demanded. The interesting questions for the fundamental study on 2D mechanical properties are not only their stiffness, Poisson's ratio, toughness, maximum intrinsic stress, fracture, adhesion, etc., but also their anisotropic and nonlinear behaviors, the reaction to thermal stress, and most importantly, how to utilize them to engineering desired nanodevises.

In this paper, we will present our recent study on the anisotropic and nonlinear mechanical properties of 2D

nanomaterials, especially, on graphene, SiC sheet, and recently predicted 2D sandwiched GaP and InP binary materials [**38**]. We performed a comprehensive computational calculation based on the state-of-the-art quantum mechanics based mothed [**39-41**] and studied the response of mechanical properties to various strains exerted on these 2D nanomaterials. We will show that these 2D materials undergo an elastic expansion-structural deformation-structural distortion process as the tensile strain increases. Such process strongly depends on the direction of the strain exerted on the 2D materials. More interesting, a phase transition was found in 2D sandwiched GaP and InP binary compounds when the strain exerts in zigzag direction. The stiffness and the nonlinear elastic moduli in graphene are greatest [**42**], followed by 2D SiC monolayer [**43**]. While the 2D III-V binary compounds, e.g., recent predicted sandwiched GaP and InP structures [**38**] possess significant anisotropic and nonlinear mechanical properties. Especially, their moduli along the zigzag direction are about 3-9 times greater than those along the armchair direction. For all 2D materials studied here, the linear elastic behavior holds only in the infinitesimal strain and the effective nonlinear elastic feature always dominates in finite strain. Such results will provide fundamental information at atomic level for further applications in material science and engineering.

Methodology

Theoretical frameworks for studying mechanical properties can be categorized into two classes: (1) modelling based on conventional continuum and structural mechanics, and (2) atomistic simulations including (i) classical molecular dynamics with empirical potentials, (ii) tight-binding methods, and (iii) first-principle quantum mechanics. In this work, we performed atomistic simulations based on the density functional theory (DFT) [**41**] and a semi-empirical method (referred as SCED-LCAO [**39, 40**]).

The deformation of a 2D structure under both in-plane and bending deformation is described through the gradient tensor F:

$$F_{iJ} = \frac{\partial x_i}{\partial X_J}; \quad i = 1,2,3; \quad J = 1,2 \tag{1}$$

where X_J and x_i are the components of the atomic coordinates before and after deformation. The infinitesimal segment $d\vec{X}$ and corresponding segment dx are related by $d\vec{x} = F d\vec{X}$. For a uniaxial stretch along X_1-direction, we have $F_{11} = \frac{\partial x_1}{\partial X_1} = \lambda; \quad F_{22} = \frac{\partial x_2}{\partial X_2} = 1;$ and other elements are zero. The nominal (tensile) strain in the X_1-direction is then introduced by $\varepsilon = \lambda - 1$, and the Green-Lagrange strain tensor E (characterizing the physical and geometrical nonlinearity feature or large deformation) is defined as

$$E_{JK} = \frac{1}{2}\left(F_{iJ} - F_{iK} - \delta_{JK}\right); \delta_{JK} = \begin{cases} 1, J = K \\ 0, J \neq K \end{cases} \tag{2}$$

The 2D nominal stress P (analogous to the first Piola-Kirchhoff Stress in 3D) can be calculated through the strain energy density function Φ:

$$P_{iJ} = \frac{\partial \Phi}{\partial F_{iJ}}; \quad \text{where} \quad \Phi = \frac{U(\varepsilon) - U(0)}{A_0} \tag{3}$$

Here, $U(\varepsilon)$, $U(0)$, and A_0 are total energy per atom at the deformation state, the total energy per atom at the equilibrium state, and the area per atoms at equilibrium, respectively. For a uniaxial stretch in the X_1-direction, for instance, P reduces to $P_{11} = \frac{\partial \Phi}{\partial \varepsilon}$.

The 2D membrane (tensile) stress S (analogous to the second Piola-Kirchhoff Stress in 3D) with respect to the Gree-Larange strain tensor E is defined as:

$$S_{IJ} = \frac{\partial \Phi}{\partial E_{IJ}} = \frac{P_{IJ}}{1 + \varepsilon}, \tag{4}$$

and for a uniaxial stretch in the X_1-direction, S_{11} will be expressed in terms of E_{11} as follows,

$$S_{11} = Y^{2D}E_{11} + D^{2D}E_{11}^2 + F^{2D}E_{11}^3 \tag{5}$$

Here, Y^{2D}, D^{2D}, and F^{2D} are the 2D Young's modulus at infinitesimal strain, the third-order, and the fourth-order (effective nonlinear) elastic moduli, respectively. The intrinsic maximum stress can be estimated at $\frac{\partial S_{11}}{\partial E_{11}} = 0$ (see Ref. [**44**] for details).

Results and discussion

A. Graphene

The anisotropic and nonlinear mechanical properties of graphene under the uniaxial tensile strain was studied in the present work. A rectangular supercell was chosen with X_1-direction along the armchair direction and X_2-direction along the zigzag direction, respectively (**Fig. 1 (a)**). The tensile strain ε was introduced by stretching the supercell along armchair/zigzag direction, and the system under different strains was fully relaxed using the SCED-LCAO method [**39, 40**]. The strain energy density function Φ (defined in Eq. (3)) along armchair and zigzag directions is then obtained from the total energy $U(\varepsilon)$ under various tensile strains and is plotted in **Fig. 1 (b)**. It can be seen that some carbon bonds parallel to the armchair direction broke and graphene is destroyed to form a series of zigzag chains as the strain exerted along armchair direction up to 0.2 (see the inset structure at the right of the upper panel in **Fig. 1 (b)**). However, no carbon bonds broke even the strain exerted on graphene along zigzag direction up to 0.23 (see the inset structure at the right of the bottom panel in **Fig. 1 (b)**), indicating the directional selectivity of graphene with response to the strain. By fitting the strain energy density function with polynomial format, one can determine the membrane stress S from Eq. (4). The results for the stress S along two directions are shown in **Fig. 1 (c)**.

(a)

(b)

(c)
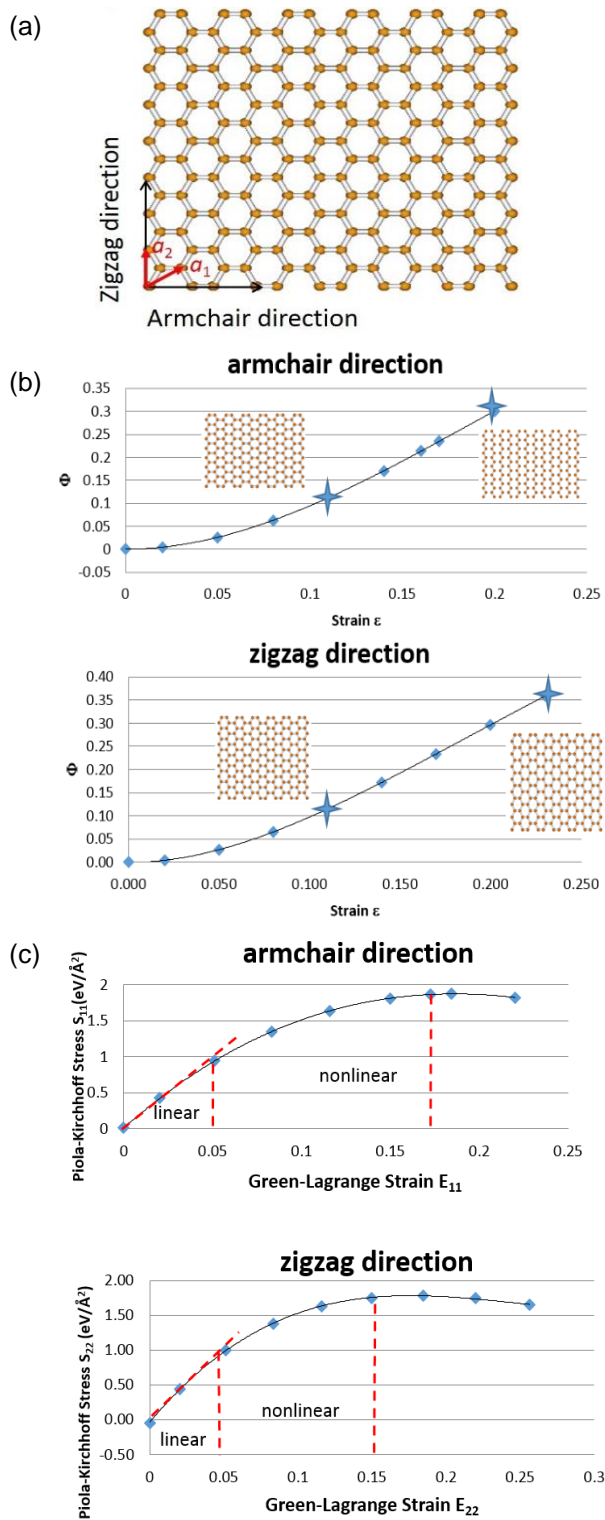
Fig. 1. (a) Schematic illustration of the rectangular supercell of graphene with the armchair and zigzag directions along the horizontal and the vertical axes, respectively. The lattices a_1 and a_2 are indicated by red arrows. (b) Obtained strain energy density function Φ as the function of the tensile strain ε along armchair (upper panel) and zigzag (bottom panel). The insets are various frameworks of graphene corresponding to the tensile strain at crosses. (c) Obtained 2D membrane stress S as the function of the strain tensor E along armchair (upper panel) and the zigzag (bottom panel), respectively. The red-dashed lines indicate the slopes, the separation between linear and nonlinear regimes, and strains at intrinsic maximum stresses, respectively.

It monotonically increases as the increase of the strain and shows a maximum at 0.17 along armchair and 0.15 along zigzag directions, respectively. The slopes of the membrane stress curves at the infinitesimal strain (*i.e.*, $E < 0.05$) indicate the linear response of graphene to the strain tensor E and provide the magnitude of the stiffness Y^{2D} (see Eq. (5)). The intrinsic maximum stress is estimated ~26.7/23.6 N/m at the strain ~0.17/0.15 for armchair/zigzag (see the right vertical dash lines in **Fig. 1 (c)**), indicating that graphene can sustain heavy load by 15-17%. The curvatures of the tensile stress demonstrate that the linear behavior dominates only at the strain less than 5% and the nonlinear behavior mainly dominate in the large range of strain.

The Young's modulus Y^{2D} at infinitesimal strain and the effective nonlinear elastic modulus D^{2D} at finite strain are obtained from Eq. (5) and are listed in **Table 1**. Both Y^{2D} and D^{2D} are greater in zigzag direction than in armchair direction, showing again the anisotropic nature in graphene. Obtained directional dependent Young's modulus is consistent with the experimental measurement [23] (the 4th row in Table 1) and other theoretical results [45-49] (rows 5-9 in Table 1). While obtained effective nonlinear elastic modulus D^{2D} is somewhat overestimated as compared to the experimental value [23]. One of the reasons might come from the temperature effect. Theoretical calculated values are obtained at 0 *K* and experimental value is measure at room temperature.

Table 1. Young's modulus Y^{2D} at infinitesimal strain (the 2nd column) and the effective nonlinear elastic modulus D^{2D} (the 3rd column) of graphene obtained by present work (rows 2 and 3) and other theoretical methods (rows 5-9) [45-49]. The experimental values [23] are also listed (the 4th row) for comparison.

Method	Y^{2D} (N/m)	D^{2D} (N/m)
Present work- Armchair	356.3	-1190
Present work- Zigzag	414.7	-1833
ab initio calculation [45]	340±40	-690±120
ab initio calculation [45]	345	—
Tersoff-Brenner calculation [46]	235	—
ab initio calculation [47]	350	—
Tight binding+ continuum elasticity theory [48]	312	-582.9
Empirical force constant model [49]	384	—

Fig. 2 shows the reaction of graphene to the thermal stress at different temperatures. When the tensile strain ε is exerted to the graphene with the strength of 0.14 along the armchair direction, the graphene still keeps its honeycomb framework at 300 K, but some of the carbon bonds began to break when the temperature is elevated to 600 K (see **Fig. 2 (a)**). While, when the strain ε is exerted to the graphene along the zigzag direction, such phenomena only occur when the tensile strain increases to ~ 0.16 at 600 K (see **Fig. 2 (a)**), indicating again the anisotropic mechanical nature of graphene under thermal stress.
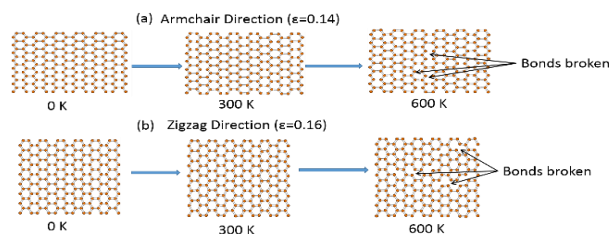
Fig. 2. Schematic illustration of the structural evolution of graphene under temperatures with the strain exerted along armchair (a) and zigzag (b), respectively.
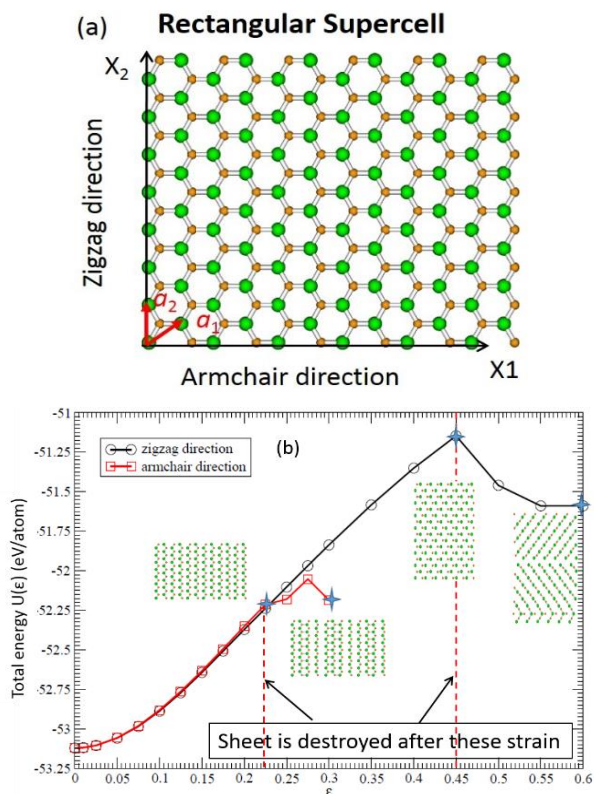
Fig. 3. (a) Schematic illustration of the rectangular supercell of 2D SiC sheet with the armchair/zigzag direction along the horizontal/vertical axis. The lattices a1 and a2 are indicated by red arrows. (b) The total strain energy per atom $U(\varepsilon)$ as the function of the tensile strain ε. The red-squares represent the strain energy along the armchair direction, and the black circles are the strain energy along the zigzag direction. The insets are the top views of SiC sheet under different strains indicated by corresponding crosses. The red-dashed lines denote structure distortion points.

B.   2D SiC sheet

The structure of the 2D SiC sheet has been predicted to be flat with hexagonal symmetry, similar to graphene but with the lattice constant of 3.08 Å [**50**]. Its anisotropic and nonlinear mechanical behavior under the uniaxial tensile stress is then expected to be similar to these of graphene. In our present work, a rectangular supercell was chosen with X_1-direction along the armchair and X_2-direction along the zigzag direction, respectively (as shown in **Fig. 3 (a)**). The strain was introduced by stretching the supercell along armchair/zigzag direction, and the system under different strains was fully relaxed using the SCED-LCAO method [**39, 40**]. **Fig. 3 (b)** shows the total strain energy per atom $U(\varepsilon)$ under the

strain ε. It is found that the SiC sheet undergoes bonds broken and then a structure distortion with zigzag chains (see the two inset structures at the left of **Fig. 3(b)**) when the strain excesses 0.22 along the armchair direction. However, if the strain is exerted along the zigzag direction, such kind of process occurs until the strain excesses 0.45 (see the two inset structures at the right of **Fig. 3(b)**), almost as twice as large in strain than that along the armchair direction, indicating that the 2D SiC sheet could sustain heavy load along the zigzag direction.

Calculated membrane stress S along the armchair and the zigzag directions are shown in **Fig. 4**. Within the allowed strain regime, the stress monotonically increases as increasing the strain and reaches its maximum at $E = \sim 0.22$ for both directions. To study its linear and nonlinear behaviors, the first-order (blue curves), second-order (green curves), and third-order (red curves) polynomial functions were used to fit the S curves. The linear elastic properties, corresponding to the Young's modulus Y^{2D}, is found to play the role only at infinitesimal strain, $i.e.$, < 0.025 along both directions. While, the nonlinear second-order elastic properties, corresponding to D^{2D}, is found to dominate mainly in the strain range of 0.025-0.08 for armchair direction and 0.025 - 0.11 for the zigzag direction.
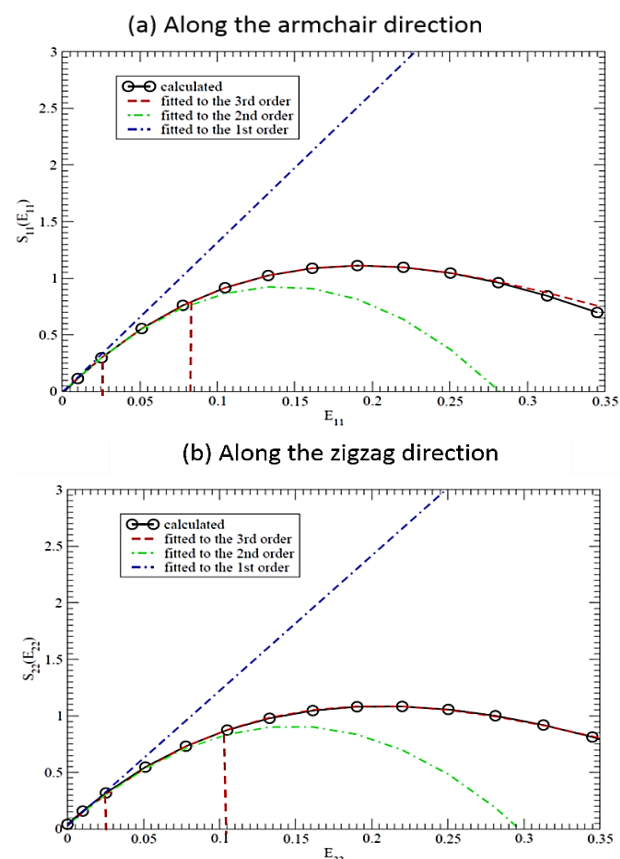
Fig. 4. Obtained 2D membrane stress S (black curves) of SiC sheet as the function of the strain tensor E along armchair (a) and zigzag (b) directions, respectively. The blue double-dash-dotted curves are the first-order fitting functions, the green dash-dotted curves are the second-order fitting functions, and the red dashed curves are the third-order fitting functions. The red-dashed vertical lines separate the linear, the quadratic, and the cubic regimes.

Calculated 2D Young's modulus Y^{2D} at the infinitesimal strain and the effective nonlinear elastic modulus D^{2D} at the finite strain regime are listed in **Table 2** and compared to other theoretical calculations [**51**] as well as the experimental measurements for bulk SiC [**52**] and amorphous SiC film [**53**]. It is found that both Y^{2D} and D^{2D} are slightly greater in armchair direction than in zigzag direction. Such anisotropic feature is opposite to that of graphene where the zigzag direction shows strong Y^{2D} and D^{2D}. Furthermore, the Young's moduli along both directions are ~56% smaller than these of graphene and the linear elastic regime is only half of that in graphene, indicating that the stiffness of SiC sheet is weak and the SiC sheet is rigid as compare to graphene. But, the estimated average stiffness of SiC sheet (~ 598 GPa) is still about 1.3 times greater than a hypothetical bulk SiC [**52**] film or 2.49 times greater than a hypothetical amorphous SiC film [**53**] of the same thickness (assuming the thickness of the SiC sheet is ~3.4 Å). Furthermore, the nonlinear behaviors are found to play the essential role when the strain is bigger than 0.025.

Table 2. Young's modulus Y^{2D} (the 2nd column) and the effective nonlinear elastic modulus D^{2D} (the 3rd column) of SiC sheet obtained from present work and other theoretical work [51]. The experimental values for bulk SiC [52] and amorphous SiC film [53] are also listed for comparison.

Method	Y^{2D} (N/m)	D^{2D} (N/m)
Present work-Armchair	208.8	-728.8
Present work- Zigzag	198.6	-681.1
Ab initio calculation [51]	166.6	—
Bulk SiC [52]	450 (GPa)	—
Amorphous SiC film [53]	240 (GPa)	—

C. 2D sandwiched GaP and InP binary compounds

Quite recently, the 2D sandwiched GaP and InP binary compounds were theoretically predicted by our group [**38**]. Comparing with the previous predicted low-buckled Gap and InP sheets [**51**], the newly predicted sandwiched GaP and InP binary compounds are energetically more stable. Its anisotropic structure (see the top and two side views at the left bottom insets in **Fig. 5 (a)-(d)**) will definitely affect their anisotropic mechanical properties. As seen from **Fig. 5** and **Fig. 6**, both GaP and InP undergo a structural deformation (in the range of $0.2 < \varepsilon < 0.33$) and then a distortion (in the range of $\varepsilon > 0.33$) when the tensile strain exerts along the armchair direction (**Fig. 5 (a)** and **Fig. 6 (a)**). Very interesting finding is that when the tensile strain exerts along the zigzag direction, the strain energy density function shows an abrupt point at $\varepsilon \sim 0.2$ and, instead of structural distortion, a phase transition from a hexagonal ring lattice to a rectangular ring lattice was found (**Fig. 5 (b)** and **Fig. 6 (b)**). This phenomenon was neither found in graphene nor in SiC sheet and is unique feature for 2D sandwiched GaP and InP binary compounds.
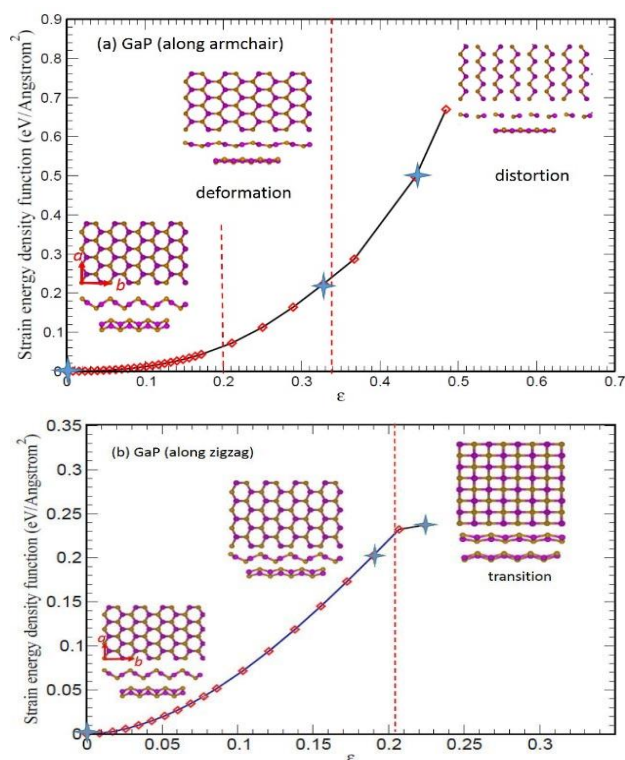
Fig. 5. The strain energy density function (calculated using the DFT method implemented in the VASP code [41]) via the tensile strain ε for GaP along armchair (a) and zigzag (b). The insets are the corresponding top and two side views of 2D sandwiched GaP binary compounds under different strains indicated by crosses. The lattices a and b are indicated by red arrows. The vertical red-dash lines represent the boundaries between different structural symmetry regimes.
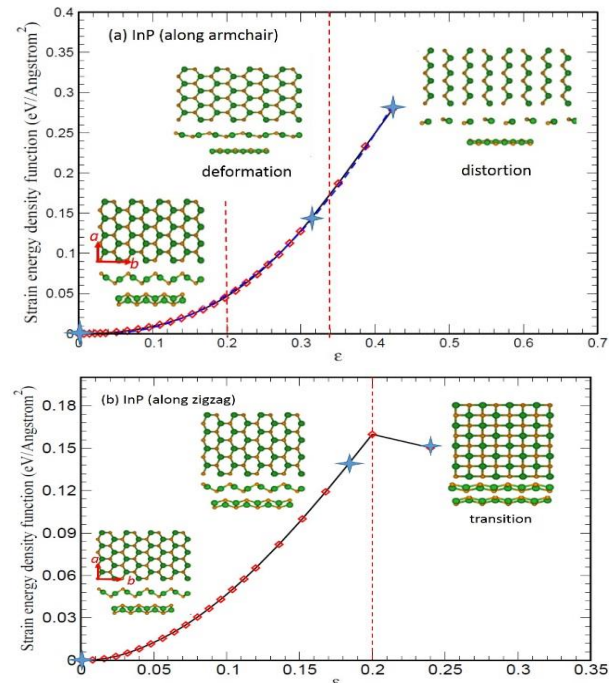
Fig. 6. The strain energy density function (calculated using the DFT method implemented in the VASP code [41]) via the tensile strain ε for InP along armchair (a) and zigzag directions (b). The insets are the corresponding top and two side views of 2D sandwiched InP binary compounds under different strains indicated by crosses. The lattices a and b are indicated by red arrows. The vertical red-dash lines represent the boundaries between different structural symmetry regimes.

The tensile stress S for the 2D sandwiched GaP and InP (black curves in **Fig. 7**) are obtained from their strain energy density function as described in Eq. (4). Corresponding uniaxial stretch along the armchair (**Fig. 7 (a)** and **(c)**) and the zigzag (**Fig. 7 (b)** and **(d)**) directions are analyzed in terms of the 1st-order (red curves), 2nd-order (green curves), and 3rd-order (blue curves) of polynomial functions. The regime for the linear response along the armchair direction ($0 < \varepsilon < 0.07$) is larger than that along the zigzag direction ($0 < \varepsilon < 0.03$). Similar trend is also found for the nonlinear response regimes. Noted that a phase transition occurs along the zigzag direction at $\varepsilon \sim 0.2$ while at the same strain, the deformation occurs along the armchair direction.
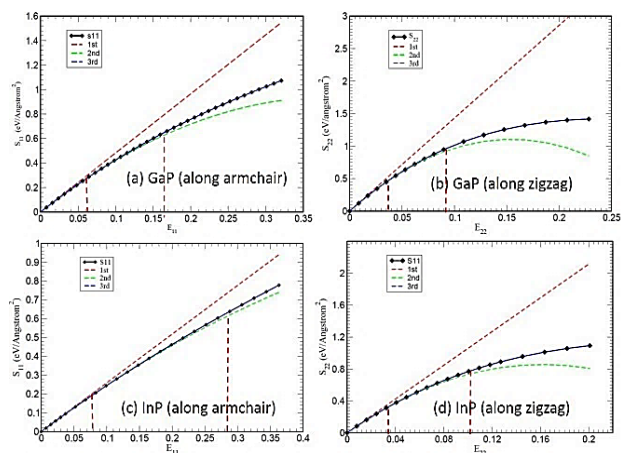
Fig. 7. Obtained 2D membrane stress S (black curves) of sandwiched GaP and InP binary compounds as the function of the strain tensor E along armchair ((a) and (c)) and zigzag ((b) and (d)) directions, respectively. The red dashed curves are the first-order fitting functions, the green dashed curves are the second-order fitting functions, and the blue dashed curves are the third-order fitting functions. The red-dashed vertical lines separate the linear, the quadratic, and the cubic regimes.

Calculated Young's modulus Y^{2D} at the infinitesimal strain and the effective nonlinear elastic modulus D^{2D} for 2D sandwiched GaP and InP binary compounds at the finite strain regime were obtained from Eq. (5) and are listed in **Table 3**. Other theoretical calculations for low buckled GaP and InP sheets [51] are also listed for comparison. The linear elastic behavior Y^{2D} holds when the strain is less than 0.03 along the zigzag, but ~0.07 along the armchair directions. The effective nonlinear elastic modulus D^{2D}, however dominate in the regimes of 0.07-0.17 (0.27) for GaP (InP) in armchair direction and 0.03-0.07 (0.09) for GaP (InP) in the zigzag direction. Different from graphene and SiC sheet, in the 2D sandwiched GaP and InP binary compounds, the stiffness Y^{2D} is ~ three times greater in the zigzag direction than in the armchair direction. Similarly, the effective nonlinear elasticity D^{2D} is ~ nine time greater in the zigzag direction as compared to those in the armchair direction, demonstrating significant anisotropic feature. The low buckled GaP and InP sheets, on the other hand, have very week stiffness [51].

Table 3. The Young's modulus Y^{2D} (the 2nd column) and the effective nonlinear elastic modulus D^{2D} (the 3rd column) of 2D sandwiched GaP and InP binary compounds calculated by present work. The theoretical calculations for low buckled GaP and InP sheets [51] are also listed for comparison.

Systems	Y^{2D} (N/m)	D^{2D} (N/m)
Sandwiched GaP - Armchair	71.81	-98.97
Sandwiched GaP - Zigzag	228.82	-741.340
Sandwiched InP - Armchair	49.67	-62.11
Sandwiched InP-Zigzag	169.21	-522.541
Low buckled GaP [51]	59	—
Low buckled InP [51]	39	—

Conclusion

The anisotropic and nonlinear mechanical properties of graphene, SiC sheet, and 2D sandwiched GaP/InP binary compounds were systemically investigated in the framework of quantum mechanics based molecular dynamics calculations [**39-41**]. Both graphene and SiC sheet have hexagonal symmetry and their anisotropic mechanical behaviors mainly come from the force that exerts either along the bonds (*e.g.*, armchair direction) or not (*e.g.*, zigzag direction). The 2D sandwiched GaP and InP binary compounds, on the other hand, have orthorhombic symmetry with pucker along the armchair direction leading to significant anisotropic mechanical properties. In particular, a new phase could be obtained by exerting force along the zigzag direction. For all 2D materials studied here, the linear elastic behavior holds only in the infinitesimal range of strain (*e.g.*, $\varepsilon < 0.05$ for graphene, $\varepsilon < 0.025$ for SiC sheet, $\varepsilon < 0.03$ for GaP/In along zigzag, and $\varepsilon < 0.07$ for GaP/InP along armchair, respectively). In the finite strain regime, the effective nonlinear elastic feature always dominates, indicating its important role played in 2D mechanical properties. It is also expected that the directional sensitivities of mechanical properties for 2D materials along any directions between the armchair and zigzag directions could be estimated within the results from the armchair and zigzag directions.

2D mechanical properties definitely affect their electronic transport properties, optical properties, and chemical properties. Alternative speaking, one can utilize their outstanding stretch ability and strength, as well as their inherent coupling of mechanical properties with other properties to design nanodevices. The strain engineering of 2D materials was established based on this principle and has been developed for a wide range of applications. For instance, a relative field-effect mobility ($\mu/\mu0$) can be produced in the flexible thin film transistor device by tuning the strain on the film [**54**]; the resistance of graphene can be varied by controlling the strain to make a graphene strain sensor [**55**]; a encapsulated graphene solution could be used for TEM measurement to protect the solution from high vacuum while being transparent to electron beams [**56**], etc. Obviously, 2D materials will be the most promising candidates for flexible and transparent electronics, sensors and composite applications [24].

Acknowledgements

Author's contributions

Conceived the plan: Ming Yu; Performed the calculations: Ming Yu, Congyan Zhang, Abdullah R Alharbi, Anna Zeng, Kevin Zeng, and Emily Liu; Data analysis: Ming Yu, Congyan Zhang, Abdullah R Alharbi, Anna Zeng, Kevin Zeng, and Emily Liu; Wrote the paper: Ming Yu (Ming Yu, Congyan Zhang, Abdullah R Alharbi, Anna Zeng, Kevin Zeng, and Emily Liu are the initials of authors). Authors have no competing financial interests.

References

1. Novoselov, K. S.; Geim, A. K.; Morozov, S. V.; Jiang, D.; Zhang, Y.; Dubonos, S. V.; Grigorieva, I. V.; Firsov, A. A.; *Science*, **2004**, *306*, 666.
2. Kagan, Cherie R.; Fernandez, Laura E.; Gogotsi, Yury; Hammond, Paula T.; Hersam, Mark C.; Nel, André E.; Penner, Reginald M. C.; Willson, Grant; Weiss, Paul S.; ACS *Nano*, **2016**, *10*, 9093.
3. Butler, S. Z.; Hollen, S. M; Cao, L.; Cui, Y.; Gupta, J. A.; Gutiérrez, H. R.; Heinz, T. F.; Hong, S. S.; Huang, J.; Ismach, A. F.; Johnston- Halperin, E.; Kuno, M.; Plashnitsa, V. V.; Robinson, R. D.; Ruoff, R. S.; Salahuddin, S.; Shan, J.; Shi, L.; Spencer, M. G.; Terrones, M.; Windl, Wolfgang; Goldberger, Joshua E.; *ACS Nano*, **2013**, *7*, 2898.
4. Topsakal, M.; Akturk, E.; Ciraci, S.; *Phys. Rev. B*, **2009**, *79* 115442.
5. Zhi, C. Y.; Bando, Y.; Tang, C. C.; Kuwahara, H.; Golberg, D.; *Adv. Mater.,* **2009**, *21*, 2889.
6. Cahangirov, S.; Topsakal, M.; Aktürk, E.; Şahin, H.; Ciraci, S.; *Phys. Rev. Letts.,* **2009**, *102*, 236804.
7. Bertolazzi, S; Brivio, J; Kis, A; *ACS Nano*, **2011**, *5*, 9703.
8. Bjorkman, T.; Gulans, A.; Krasheninnikov, A. V.; Nieminen, R. M.; *Phys. Rev. Lett.*, **2012**, *108*, 235502.
9. Bernardi, M.; Palummo, M.; Grossman, J. C.; *Nano Lett*., **2013**, *13*, 3664.
10. Liu, H; Neal, A. T.; Zhu, Z.; Luo, Z.; Xu, X. F.; Tomanek, D.; Ye P. D.; ACS *Nano*, **2013**, *8*, 4033.
11. Lu, W. L.; Nan, H. Y.; Hong, J. H.; Chen, Y. M.; Zhu, C.; Liang, Z.; Ma, X. Y.; Ni, Z. H.; Jin, C. H.; Zhang, Z.; *Nano Res.,* **2014**, *7*, 853.
12. Buscema, M.; Groenendijk, D. J.; Blanter, S. I.; Steele, G. A.; *Nano Lett*., **2014**, *14*, 3347.
13. Naguib, M.; Mochalin, V.N.; Barsoum, M.W.; Gogotsi, Y; *Advanced Materials*, **2011**, *26*, 992.
14. Naguib, M.; Kurtoglu, M.; Presser, V.; Lu, J.; Niu, J.; Heon, M.; Hultman, L.; Gogotsi, Y.; Barsoum, M.W.; *Advanced Materials*, **2011**, *23*, 4248.
15. Nevalaita, Janne; Koskinen Phys, Pekka; *Phys. Rev. B*, **2018**, *97*, 035411.
16. Lei, Lijun; Wu, Zhiwei; Liu, Huan; Qin, Zhangfeng; Chen, Chengmeng; Luo, Li; Wang, Guofu; Fan, Weibin; Wang, Jianguo; *J. Mater. Chem. A,* **2018**, *6*, 9948.
17. Evans, David G.; Slade, Robert C. T.; *Structure and Bonding,* **2006**, *119*, 1.
18. Diercks, Christian S.; Yaghi; Omar M.; *Science,* **2017**, 355, 923.
19. Batten, S. R.; Champness, N. R.; Chen, X. M.; Garcia-Martinez, J; Kitagawa, S.; Öhrström, L.; O'Keeffe, M.; Suh, M. P.; Reedijk, J.; Pure *and Applied Chemistry*, **2013**, *85*, 1715.
20. Kang, Jiahao; Cao, Wei; Xiem, Xuejun; Sarkar, Deblina; Liu, Wei; Banerjee, Kaustav; *Proc. SPIE*, **2014**, *9083*, 908305.
21. Xia, Fengnian; Wang, Han; Xiao, Di; Dubey, Madan; Ramasubramaniam, Ashwin; *Nature Photonics,* **2014**, *8*, 899.
22. Ng, Leonard W. T.; Hu, Guohua; Howe, Richard C. T.; Zhu, Xiaoxi; Yang, Zongyin; Jones, Christopher G.; Hasan, Tawfique; Printing of Graphene; Related 2D Materials; Springer, Cham, Online ISBN 978-3-319-91572-2, **2018**
23. Lee, Changgu; Wei, Xiaoding; Kysar, Jeffrey W.; Hone, James; *Science*, **2008**, *321*, 385
24. Kim, Jong Hun; Jeong, Jae Hwan; Kim, Namwon; Joshi, Rakesh; Lee, Gwan-Hyoung; *J. Phys. D: Appl. Phys.*, **2019**, *52*, 083001.
25. Picas, L.; Milhiet, P. E.; Hernandez-Borrell, J.; *Chem. Phys. Lipids*., **2012**, *165*, 845.
26. Ozkan, T.; Naraghi, M.; Chasiotis, I.; *Carbon*, **2010**, *48*, 239.
27. Arshad. S. N.; Naraghi, M.; Chasiotis, I.; *Carbon*, **2011**, *49*, 1710.
28. Koenig, S. P.; Boddeti, N. G.; Dunn, M. L.; Bunch, J. S.; *Nat. Nanotechnol*., **2011**, *6*, 543.
29. Williams, J. G.; *Int. J. Fract.*, **1997**, *87*, 265.
30. Wan, N.; Pan, W.; Lin, T.; *Phys. Chem. Chem. Phys*., **2016**, *18*, 16641.
31. Lee, J. U.; Yoon, D.; Cheong, H.; *Nano Lett*., **2012**, *12*, 4444.
32. Liu, Z.; Yang, J.; Grey, F.; Liu, J. Z.; Liu, Y.; Wang, Y.; Yang, Y.; Cheng, Y.; Zheng, Q.; *Phys. Rev. Lett.*, **2012**, *108*, 205503.
33. Zheng, Q.; Jiang, B.; Liu, S.; Weng, Y.; Lu, L.; Xue, Q.; Zhu, J.; Jiang, Q.; Wang, S.; Peng, L.; *Phys. Rev. Lett.,* **2008**, *100*, 067205.
34. Lee, J. H.; Loya, P. E.; Lou, J.;, Thomas, E. L.; *Science*, **2014**, *346*, 1092.
35. Mate, C. M.; McClelland, G. M.; Erlandsson, R.; Chiang, S.; Scanning Tunneling Microscopy (Berlin: Springer), **1987**, pp 226–9.
36. Bennewitz, R.; Fundamentals of Friction and Wear on the Nanoscale (Berlin: Springer), **2015**, pp 3–16.
37. Meyer, E.; Lüthi, R.; Howald, L.; Güntherodt, H. J.; Forces in Scanning Probe Methods (Berlin: Springer), **1995**, pp 285–306.
38. Zhang, Congyan Yu, Ming; *Nanotechnology*, **2018**, 29, 095703.
39. Yu, Ming; Wu, S.Y; Jayanthi, C.S.; *Physica E*, **2009**, *42,* 1.
40. Leahy, C.; Yu, M.; Jayanthi, C.S.; Wu, S.Y.; *Phys. Rev. B*, **2006**, *74*, 155408.
41. Kresse, G.; Furthmuller, J.; *Phys. Rev. B*, **1996**, *54*, 11169.
42. Yu, M.; Zeng, Anna; Zeng, Kevin; Abstracts of paper, Session 12.1.1: Graphene: Synthesis, Defects, and Properties, March Meeting, American Physical Society, Bulletin of Annual Meeting of APS, **2014**, Vol. 59, 189.
43. Yu, Ming; Liu, Emily; Zhang, Congyan; Abstracts of paper, Session 12.1.6: Computational Discovery and Design of New Materials, March Meeting, American Physical Society, Bulletin of Annual Meeting of APS, **2015**, Vol. 60, 329.
44. Lu, Qiang; Huang, Rui; *International Journal of Applied Mechanics*, **2009**, *1*, 443.
45. Kudin, K. N.; Scuseria, G. E.; Yakobson, B. I.; *Phys. Rev. B*, **2001**, *64*, 235406.
46. Zhou, J.; Huang, R. J.; *Mech. Phys. Solids*, **2008**, *56*, 1609.
47. Liu, F; Ming, P.M.; Li, J.; *Phys. Rev. B*, **2007**, 76, 064120-064127.
48. Cadelano, E.; Palla, P.L.; Giordano, S.; Colombo, L.; *Phys. Rev. Let*t., **2009**, *102*, 235502.
49. Michel, K. H.; Verberck, B.; P*hys. Stat. Sol. (b)*, **2008**, *245*, 2177.
50. Yu, Ming; Jayanthi, C. S.; Wu, S. Y.; *Phys. Rev. B*, **2010**, *82*, 075407.
51. Şahin, H.; Cahangirov, S.; Topsakal, M.; Bekaroglu, E.; Akturk, E.; Senger, R.T.; Ciraci1, S.; Phys. *Rev. B*, **2009**, *80*, 155453.
52. Elastic Properties and Young Modulus for some Materials, The Engineering Tool Box (Retrieved 2012-01-06), **2012** (https://www.engineeringtoolbox.com/young-modulus-d_417.html)
53. Khakani, M. A. El; Chaker, M.; Jean, A.; Boily, S.; Kieffer, J. C; *J. Mater. Res.*, **1994**, *9*, 96.
54. Lee, G. H.; Yu, Y. J.; Cui, X.; Petrone, N.; Lee, C.H.; Choi, M.S.; Lee, D.Y.; Lee, C.; Yoo, W.J.; Watanabe, K.; Taniguchi, T.; Nuckolls, C.; Kim, P.; Hone, J.; *ACS Nano*. **2013**, *7*, 7931.
55. Berinskii, I. E.; Indeitsev, D. I.; Morozov, N. F.; Skubov, D. Y.; Shtukin, L. V.; *Mech. Solids,* **2015**, *50*, 127.
56. Yuk, J. M.; Park, J.; Ercius, P.; Kim, K.; Hellebusch, D. J.; Crommie, M. F.; Lee, J. Y.; Zettl, A.; Alivisatos, A. P.; *Science,* **2012**, *336*, 61.